Robotica (2011) volume 29, pp. 445–459. © Cambridge University Press 2010
doi:10.1017/S0263574710000287

Numerical synthesis of three-dimensional gait cycles by dynamics optimization

Tarik Saidouni

Laboratory of Structure Mechanics, Polytechnics Military School, BP 17 Bordj El Bahri 16046, Algiers, Algeria

(Received in Final Form: June 9, 2010. First published online: July 7, 2010)

SUMMARY

The present paper aims at generating three-dimensional cyclic gait of a biped with a locomotion system having anthropomorphic characteristics. Kinematic and dynamic models of both single and double support phases are extensively developed with a special attention devoted to the double support phase. A variety of gait constraints defining a feasible walk is taken into account. Joint trajectories are approximated by cubic spline functions connected at uniformly distributed knots. Joint coordinates at knots, walking phase durations, and independent parameters at phase transitions are the design parameters of a parametric optimization problem. Therefore, only the pattern organization and the gait speed are explicitly specified. The effectiveness of the proposed method is verified and discussed through some simulation results.

KEYWORDS: 3D-gait synthesis; Walking dynamics; Anthropomorphic biped; Parametric optimization.

1. Introduction

Significant advances in humanoid robotics have been achieved during the past few years. Today, sophisticated robot platforms such as ASIMO,[1] HRP-3,[2] and JOHNNIE[3] confirm the feasibility of bipedal walking machines. A frequently used approach for designing a full biped control scheme is to combine an *a priori* definition of desired trajectories to be followed, a classical control allowing them to be tracked and a dedicated online adaption technique to cope with model uncertainties and disturbances to prevent the robot from falling.[4–6] The current humanoids use several times more energy than passive biped robots or human beings because of generated patterns and online controls of a humanoid are mainly devoted to ensuring the dynamical stability using simplified multibody system models.[7,8] They do not take advantage of their inherent dynamics which allows, under some conditions, passive-dynamics gait or intermittent and small active power gait.[9,10]

The desired patterns or reference trajectories can be purely computer-generated. An interesting way of achieving this computation is to use an optimization algorithm based on the dynamics and taking into account various physical constraints, such as the dynamic stability, hard to achieve because of intrinsic instability of bipeds. Gait dynamic optimization, aimed both at improving the biped control and reducing energy expenditure, results therefore in increasing the autonomy and making progress in locomotion efficiency of future humanoid robots. Moreover, as centuries of evolution have improved human walking to near optimality, it is expected that interesting characteristics of human gaits, such as quasi-passive walking, can be retrieved indirectly by motion optimization based on an accurate dynamics model of a human being and using appropriate criteria. The optimization approaches can also be useful for other objectives, such as the biped actuator sizing during the design process and the inverse dynamics model solving in biomechanics.[11]

Most of the papers that deal with gait dynamic optimization are mainly dedicated to the sagittal movements especially during the swing phase.[12–14] A method for generating optimal cyclic sagittal gait, composed by a single support phase (SSP) and a double support phase (DSP), is proposed in ref. [15] for a biped modelled as a seven-link planar mechanical system. Thus, the characteristic curves, such as energy consumption, average power and step lengthening variations of the planar model of the bipedal robot BIP[16] have been established in the case of the impactless walking.[17] The proposed approach is based on approximating generalized coordinates using spline functions of class C^2. Later, a similar parametric optimization approach,[18] using third-order differentiable approximation functions, was considered. This avoids jerky variations of the contact forces and actuating torques. Nevertheless, the continuity of the contact forces and the actuating torques between the gait phases has not been fulfilled.

However, accurate modelling of both robot kinematics and dynamics requires introducing two other planes, the frontal and the transversal planes. Although this three-dimensional (3D) model is particularly crucial for the development of dynamically stable and smooth gaits, we deal with more complex problem compared to the sagittal model. It leads to a high-dimensional, nonlinear, and complex mathematical modelling. For this reason, we proposed as a first attempt in ref. [19] a method for combining sagittal gait with sway motion in the frontal plane for the three-dimensional walk during the SSP. The model obtained in this way was an approximation of real walk. These simplifications allow analyzing some of the predominant behaviors of walking dynamics, but many other features are lost.

In the framework of studying the biomechanics of human locomotion, offline generation of 3D-gait was considered in ref. [20]. The proposed method for motion planning was tested on a simplified virtual human, which is modelled as

* Corresponding author. E-mail: Tarik.Saidouni@gmail.com

https://doi.org/10.1017/S0263574710000287 Published online by Cambridge University Press

a multibody system with 25 degrees of freedom (DOFs). By combining inverse dynamics and optimization, this method involves actuating torques neither in the constraints nor in the performance index in order to avoid computation complexity. The resulting motion is not optimal in terms of energy expenditure making its usefulness limited. In refs. [21, 22], optimal control problems have been proposed for optimal 3D-gait generation. The solution is obtained by using the direct collocation method implemented in the DIRCOL code.[23] The controls are approximated using linear interpolation functions, whereas the states are chosen as continuously differentiable functions. The approximation points on the controls and the configuration variables are the nonlinear program parameters where complementary equality constraints are added to take into account the dynamics at discretization points.

In this paper, we propose a different approach based on the discretization of only the configuration variables via a cubic spline approximation from which input controls are deduced exactly using the inverse dynamics models. Consequently, the correlation between the system states and their controls is implicitly and constantly accurate. With this approach, globally optimized three-dimensional straight-ahead gaits can be generated where neither gait phases durations nor step-length and step-width are specified. This proposed approach can be applied to any anthropomorphic biped model (model of biped with a locomotion system having human being characteristics). It allows a broader understanding of optimal walking dynamics and provides quality reference gait trajectories for an implementation on humanoid controllers.

In Section 2 of this paper, the three-dimensional biped model and the organization of the gait patterns are described. As a result, a set of free parameters defining the DSP and the phase transitions is identified. In Section 3, complete dynamic models of both gait phases are stated and solved with respect to joint actuating torques. A special attention is given to the DSP. In Section 4, the constraints specifying the feasible walk are formulated. The parameterized optimization problem is stated in its final form in Section 5. Numerical results are presented in Section 6, and some general observations are discussed in Section 7. Finally, Section 8 concludes the paper.

2. Kinematic Model of a 3D Biped

The synthesized gait depends on the models adopted for the kinematic arrangement of the locomotion system as well as the gait organization assumptions, particularly the ground/feet contacts.

2.1. Three-dimensional locomotion system kinematic model

The anthropomorphic biped considered here is composed of two legs, each one having six joints. Three of the joints are located in the hip, one actuates the knee and another two actuate the ankle (in sagittal and frontal planes). Although actual humanoid robots have different leg mechanisms and outlooks, they are fully actuated and share these common features in their locomotion system.[1–3] Moreover, their last versions have a waist joint with up to three supplementary rotational active joints bringing several advantages for the walking dynamics.

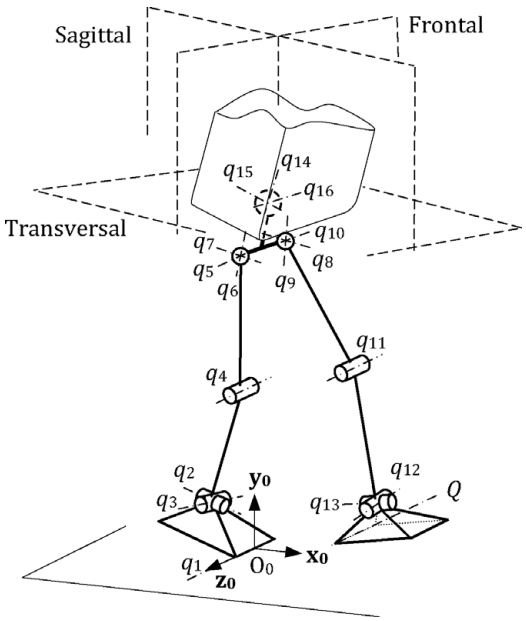


Fig. 1. Three-dimensional generic model of a biped locomotion system.

Therefore, a generic locomotion system that consists of $n = 16$ (including a passive joint coordinate q_1) joints multibody system, arranged as illustrated in Fig. 1, is considered in this paper.

A walking biped is a rooted rigid multibody system. Its architecture can be fully described by the Denavit–Hartenberg (DH) notation modified by Khalil and Kleinfinger, and presented in ref. [24]. The latter extends the familiar DH notation to describe kinematic tree-structures. Once the constant DH parameters are given, the configuration and the walking patterns of the biped are fully defined by its n DH variable parameters regrouped in the configuration parameters vector or the joint coordinates vector $\mathbf{q} = (q_1, \ldots, q_{16})^T$.

2.2. Gait phases definition

We look for a symmetric straight-ahead walking of successive and repeatable steps of length l_S, width w_S, and a zero step-angle, as shown in Fig. 2. One human-like gait cycle includes two steps. Each step exhibits a time-varying topology defining two successive phases. The SSP starts at the beginning of first step. The rear foot leaves the ground, and swings toward its new location. The biped moves as a rooted tree-like multibody system with the stance foot flat on the ground.

At instant t_{SS}, the swing foot heel touches the ground; the SSP finishes and the DSP begins. Then, both feet are in contact with the supporting ground and the locomotion system works as a closed-loop kinematic system. At DSP beginning, the rear foot is flat on the ground, and the front foot is in linear contact at heel. It is assumed that during the whole phase both feet are pivoting. The first rotates around its toe while the second rotates around its heel.

https://doi.org/10.1017/S0263574710000287 Published online by Cambridge University Press

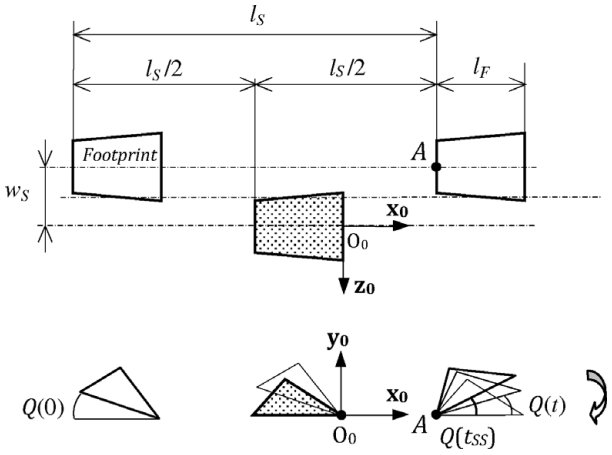


Fig. 2. Successive footprint placements (lateral and upside views).

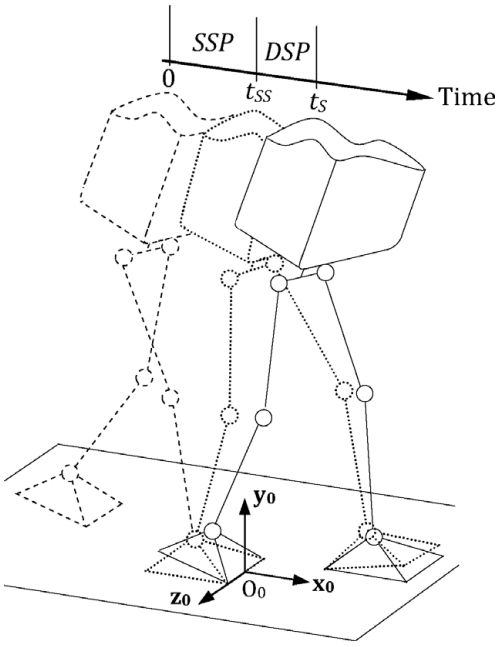


Fig. 3. Phase transition postural configurations of a step and their corresponding timing.

At instant t_S, the front foot is flat on the ground; the DSP as well as the first step are ended. The second step is bilaterally symmetric to the first one and can be readily deduced. Therefore, the gait step includes three-phase transition configurations, each one having both feet in contact with the ground as displayed in Fig. 3.

2.3. Closed-loop constraints

At three-phase transition configurations, likewise during the whole DSP, the closed-loop kinematic chain introduces constraint equations between both legs joint position variables uniquely (without the waist ones), that are grouped in the vector $\mathbf{q_C} = (q_1, \ldots, q_{13})^T$. The kinematic closed-loop results in the reduction of the locomotion system DOF, $\mathbf{q_C}$ components can be partitioned into independent $\mathbf{q_{Ci}} = (q_1, \ldots, q_7)^T$ and dependent joint coordinates $\mathbf{q_{Cd}} = (q_8, \ldots, q_{13})^T$.

Knowing the left-foot pose parameters, which are w_S, l_S, and its time-dependent orientation angle $Q(t)$ as well

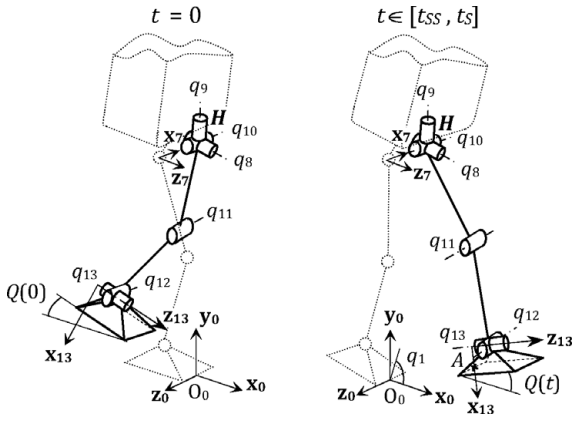


Fig. 4. Illustration of the left-leg-dependent joint coordinates.

as the independent joint coordinates $\mathbf{q_{Ci}}$, the remaining joint coordinates in $\mathbf{q_{Cd}}$ are the closed-form solution of an inverse kinematic problem similar to a 6-DOF anthropomorphic manipulator closed-form solution depicted in Fig. 4. Fortunately, among the several solutions, only one solution remains within the joint bounds, and is found by the following successive identifications:

$$\begin{cases} {}^{13}\mathbf{H}(q_{11}, q_{12}, q_{13}) = {}^{13}\mathbf{T}_0\,(w_S, l_S, Q)\ {}^{0}\mathbf{T}_7\,(\mathbf{q_{Ci}})\ {}^{7}\mathbf{H}, \\ {}^{10}\mathbf{T}_7(q_8, q_9, q_{10}) = {}^{10}\mathbf{T}_{13}\,(q_{11}, q_{12}, q_{13})\ {}^{13}\mathbf{T}_0(w_S, l_S, Q)\ {}^{0}\mathbf{T}_7(\mathbf{q_{Ci}}), \end{cases} \tag{1}$$

where the matrices ${}^{j}\mathbf{T}_i(\ldots)$ in Eq. (1) denote the 4×4-dimension homogeneous transformation matrices of modified DH parameters that transform vectors from coordinate frame number i to coordinate frame number j. ${}^{k}\mathbf{H}$ is the homogeneous coordinates vector of the left hip joint center expressed in the coordinate frame number k. As with the joint positions, joint velocities and joint accelerations are also dependent. The front foot twist (six-dimensional array defining the Cartesian velocities), reduced at a point A of the heel, having only one nonzero element (the Z-component of the angular velocity), is related to the joint velocity vector $\dot{\mathbf{q}}_\mathbf{C}$ by the following equation:

$$\begin{bmatrix} \mathbf{0} \\ \dot{Q} \end{bmatrix} = \mathbf{J}\ \dot{\mathbf{q}}_\mathbf{C}, \tag{2}$$

where $\mathbf{J}$ is the 6×13 Jacobian matrix mapping the joint velocities of both legs into the front foot twist at the point A.

The right-hand side of Eq. (2) can be written as the sum of two terms regrouping, respectively, the independent and the dependent joint velocity variables as follows:

$$\begin{bmatrix} \mathbf{0} \\ \dot{Q} \end{bmatrix} = \mathbf{J_i}\ \dot{\mathbf{q}}_{\mathbf{C}i} + \mathbf{J_d}\ \dot{\mathbf{q}}_{\mathbf{C}d}, \tag{3}$$

where $\mathbf{J_i}$ and $\mathbf{J_d}$ are 6×7- and 6×6-dimensional matrices, respectively.

Expression (3) is readily rearranged, and for a given angular velocity $\dot{Q}(t)$, the joint velocities of front leg are

https://doi.org/10.1017/S0263574710000287 Published online by Cambridge University Press

calculated by the expression

$$\dot{\mathbf{q}}_{\mathbf{C}d} = \mathbf{J_d}^{-1}\left(\begin{bmatrix}\mathbf{0}\\ \dot{Q}\end{bmatrix} - \mathbf{J_i}\,\dot{\mathbf{q}}_{\mathbf{C}i}\right). \tag{4}$$

In order to compute the joint accelerations, both sides of Eq. (2) are differentiated with respect to time, which yields to

$$\begin{bmatrix}\mathbf{0}\\ \ddot{Q}\end{bmatrix} = \mathbf{J}'\,\dot{\mathbf{q}}_{\mathbf{C}} + \mathbf{J}\,\ddot{\mathbf{q}}_{\mathbf{C}}, \tag{5}$$

where $\mathbf{J}'$ stands for the Jacobian time-derivative.

The decomposition of the Jacobian matrix $\mathbf{J}$ as in Eq. (3) gives

$$\begin{bmatrix}\mathbf{0}\\ \ddot{Q}\end{bmatrix} = \mathbf{J}'\,\dot{\mathbf{q}}_{\mathbf{C}} + \mathbf{J_i}\,\ddot{\mathbf{q}}_{\mathbf{C}i} + \mathbf{J_d}\;\ddot{\mathbf{q}}_{\mathbf{C}d}. \tag{6}$$

Finally, the joint accelerations of the front leg can be computed as follows:

$$\ddot{\mathbf{q}}_{\mathbf{C}d} = \mathbf{J_d}^{-1}\left(\begin{bmatrix}\mathbf{0}\\ \ddot{Q}\end{bmatrix} - \mathbf{J}'\,\dot{\mathbf{q}}_{\mathbf{C}} - \mathbf{J_i}\,\ddot{\mathbf{q}}_{\mathbf{C}i}\right). \tag{7}$$

During the DSP, the front foot angular motion $Q(t)$ is prescribed by a quintic polynomial:

$$\forall t \in [t_{SS},\ t_S], \qquad Q(t) = \sum_{i=0}^{5} a_i\, t^i. \tag{8}$$

The six polynomial coefficients a_i are deduced from six constraint conditions on the position, the velocity, and the acceleration. Indeed, knowing $\mathbf{q}_{\mathbf{C}}$, at the SSP end, and its first two time-derivatives, the first three constraint equations are such that

$$\begin{cases} Q(t_{SS}) = F_6\left(\mathbf{q}_{\mathbf{C}}(t_{SS})\right),\\ \dot{Q}(t_{SS}) = [\mathrm{J}_{6,1,\ldots,13}]\,\dot{\mathbf{q}}_{\mathbf{C}}(t_{SS}),\\ \ddot{Q}(t_{SS}) = [\mathrm{J}_{6,1,\ldots,13}]'\,\dot{\mathbf{q}}_{\mathbf{C}}(t_{SS}) + [\mathrm{J}_{6,1,\ldots,13}]\,\ddot{\mathbf{q}}_{\mathbf{C}}(t_{SS}), \end{cases} \tag{9}$$

where F_6 is a nonlinear function of $\mathbf{q}_{\mathbf{C}}$ components, while $[\mathrm{J}_{6,1,\ldots,13}]$ is the sixth row of the Jacobian.

At the DSP end, the front foot becomes motionless and flat on the ground without slamming its sole, and hence the three other constraint equations are given by

$$Q(t_S) = \dot{Q}(t_S) = \ddot{Q}(t_S) = 0. \tag{10}$$

Therefore, $Q(t)$ and its two first derivatives being known at each instant of the DSP, the velocity, and the acceleration of the dependent joints are effectively given by Eqs. (4) and (7), respectively.

2.4. Set of independent parameters defining the transition postural configurations

According to the modified DH notation, the cyclic and the bilaterally symmetric character of the gait results in the following permutation relationships:

$$\begin{cases} q_1(t_S) = Q(t_{SS}),\\ q_2(t_S) = q_{13}(0),\ q_{13}(t_S) = q_2(0),\\ q_3(t_S) = -q_{12}(0),\ q_{12}(t_S) = -q_3(0),\\ q_4(t_S) = -q_{11}(0),\ q_{11}(t_S) = -q_4(0),\\ q_5(t_S) = \pi - q_{10}(0),\ q_{10}(t_S) = \pi - q_5(0),\\ q_6(t_S) = q_9(0) - \pi,\ q_9(t_S) = \pi + q_6(0),\\ q_7(t_S) = q_8(0),\ q_8(t_S) = q_7(0),\\ q_{14}(t_S) = -q_{14}(0),\\ q_{15}(t_S) = \pi - q_{15}(0),\\ q_{16}(t_S) = q_{16}(0). \end{cases} \tag{11}$$

These equalities together with the dependent joint coordinates $\mathbf{q}_{\mathbf{C}d}$ reduce the number of parameters defining the three transition postural configurations of Fig. 3 to 22 parameters, listed as follows:

$$\mathbf{x}_B = \{l_S, w_S, Q(0), Q(t_{SS}), q_i(0), q_i(t_{SS}),\ i = 2, \ldots, 7, 14, 15, 16\}. \tag{12}$$

3. Dynamic Models

The differences in kinematic structure, for each of the above gait phases, call for a specific dynamic modelling.

3.1. SSP model

Since the biped moves as a tree kinematic chain, the motion equations may be written in the following form

$$\tau = \mathbf{M}(\mathbf{q})\ddot{\mathbf{q}} + \mathbf{B}(\mathbf{q}, \dot{\mathbf{q}}) + \mathbf{G}(\mathbf{q}), \tag{13}$$

where $\mathbf{M}$ is the 16×16 symmetric and positive-definite generalized mass matrix, the vector $\mathbf{B}$ regroups Coriolis and centrifugal terms, and $\mathbf{G}$ is the vector of gravity terms.

The joint torques τ are computed from the joint motion variables, namely $\mathbf{q}$, $\dot{\mathbf{q}}$, and $\ddot{\mathbf{q}}$. The solution of this inverse dynamic problem is computationally costly, particularly, when it has to be repeated thousand times in an optimization code. Therefore, although relation (13) illustrates several sorts of forces acting on the joint torques, the general solution of the inverse dynamic problem is based on the Newton–Euler (NE) approach using the well-known and efficient recursive Newton–Euler algorithm (RNEA).[25,26]

This algorithm is composed of two parts. The link velocities and accelerations are first computed though an outward recursion from the fixed base to the tree extremity links. Having the accelerations of the mass centre of each link, the NE equations are applied to compute the inertia wrenches (force and moment vectors) during this recursion. A second, inward recursion uses the wrench balance equation based on a free body diagram at each link to compute the constraint wrenches (the reaction forces and moments at joints) that include the joint torques.

Thus, differently to the Lagrangian approach, this algorithm computes the constraint wrenches that are the joint forces $\mathbf{F_i}$ and the moments $\mathbf{M_i}$ exerted on link i by link $i-1$

https://doi.org/10.1017/S0263574710000287 Published online by Cambridge University Press

toward the stance foot. Consequently, the actuating torque vector $\mathbf{u} = (\tau_2, \ldots, \tau_{13})^T$ as well as the stance foot/ground contact force $\mathbf{F_1}$ and moment $\mathbf{M_1^{O_0}}$ are readily determined.

3.2. The DSP model

During the DSP, the biped locomotion system is equivalent to an overactuated[27] closed-loop mechanism (closed kinematic chain driven by more actuators than required). The loop-closure constraints and the overactuation exhibit more complicated dynamics than for kinematic trees.

The dynamic formulation is based on the transformation of the closed-loop system into an unconstrained spanning tree one. To make the locomotion system open, the closed-loop is cut at the front foot–ground contact "joint" such that the resulting spanning tree will be governed by the SSP dynamic Eq. (13). The removed constraints due to the cut joint are reintroduced through the Lagrange multipliers.[28]

The front foot–ground contact permits the foot rotation around an axis parallel to $\mathbf{z_0}$ passing through the point A of the heel. The principle of virtual work states that the virtual work of the constraint forces is zero.[29] In other words, the contact forces and moments act uniquely where the joint degrees of freedom are restricted. Hence, only the nonzero components of contact force $\mathbf{F_L} = (F_{L,x}, F_{L,y}, F_{L,z})^T$, and contact moment at the point A, $\mathbf{M_L^A} = (M_{L,x}^A, M_{L,y}^A, 0)^T$, form the Lagrange multipliers vector $\lambda = (F_{L,x}, F_{L,y}, F_{L,z}, M_{L,x}^A, M_{L,y}^A)^T$.

The contact efforts vector λ are propagated at all joints through the Jacobian matrix. The constrained equations of motion can be expressed in the following form:

$$\tau = \mathbf{u} + \begin{bmatrix} [\mathrm{J}_{1,\ldots,5,1,\ldots,13}]^T \\ \ldots \\ \mathbf{0}_{3\times 5} \end{bmatrix} \lambda. \tag{14}$$

Here, $\mathbf{u}$ is the actuating torques vector for the DSP, $[\mathrm{J}_{1,\ldots,5,1,\ldots,13}]$ is a 5×13 submatrix including the first five rows of the Jacobian $\mathbf{J}$, $\mathbf{0}_{3\times 5}$ is a 3×5-dimensional matrix of zeros, and τ is the torques in the spanning tree computed thanks to the RNEA.

The first component of $\mathbf{u}$ in Eq. (14) is set equal to zero because of the passive joint associated to the coordinate q_1. The foregoing expression can explicitly be written as follows:

$$\begin{bmatrix} \tau_1 \\ \tau_2 \\ \vdots \\ \tau_{13} \\ \ldots \\ \tau_{14} \\ \tau_{15} \\ \tau_{16} \end{bmatrix} = \begin{bmatrix} 0 \\ u_2 \\ \vdots \\ u_{13} \\ \ldots \\ u_{14} \\ u_{15} \\ u_{16} \end{bmatrix} + \begin{bmatrix} [\mathrm{J}_{1,\ldots,5,1,\ldots,13}]^T \\ \ldots \\ \mathbf{0}_{3\times 5} \end{bmatrix} \lambda. \tag{15}$$

This expression is split into two parts. First, the actuating torques in the kinematic branch tree corresponding to the trunk, where no external forces are applied, are directly obtained. Namely,

$$u_i = \tau_i \quad i = 14, 15, 16. \tag{16}$$

Second, the dynamics of the closed loop (ground–rear leg–front leg–ground) is formulated via the following expression:

$$\begin{bmatrix} \tau_1 \\ \tau_2 \\ \vdots \\ \tau_{13} \end{bmatrix} = \begin{bmatrix} 0 \\ u_2 \\ \vdots \\ u_{13} \end{bmatrix} + [\mathrm{J}_{1,\ldots,5,1,\ldots,13}]^T \lambda. \tag{17}$$

From the first line of Eq. (17), the spanning tree torque acting on the first joint is given by

$$\tau_1 = [\mathrm{J}_{1,\ldots,5,1}]^T \lambda. \tag{18}$$

Recall that $\mathbf{J}$ is defined as the concatenation of column matrices:[30]

$$\mathbf{J_i} = \begin{bmatrix} \mathbf{z_{i-1}} \times \overrightarrow{\mathrm{O}_{i-1}A} \\ \mathbf{z_{i-1}} \end{bmatrix} \quad \text{for } i = 1 \text{ to } 13.$$

In particular, we have

$$\mathbf{J}_1 = [\mathrm{J}_{1,\ldots,6,1}]^T = \begin{bmatrix} \mathbf{z_0} \times \overrightarrow{\mathrm{O}_0 A} \\ \mathbf{z_0} \end{bmatrix} = \begin{bmatrix} \mathrm{J}_{21}\, \mathbf{y_0} \\ \mathbf{z_0} \end{bmatrix} = (0, \mathrm{J}_{21}, 0, 0, 0, 1)^T.$$

Hence, the scalar product in Eq. (18) gives the normal force acting on the front foot as follows:

$$F_{L,y} = \tau_1 / \mathrm{J}_{21}, \tag{19}$$

and Expression (17) takes the form

$$\begin{bmatrix} \tau_2 \\ \vdots \\ \tau_{13} \end{bmatrix} = \begin{bmatrix} u_2 \\ \vdots \\ u_{13} \end{bmatrix} + \begin{bmatrix} [\mathrm{J}_{1,2,\ldots,13}]^T & [\mathrm{J}_{3,\ldots,5,2,\ldots,13}]^T \end{bmatrix} \begin{bmatrix} F_{L,x} \\ F_{L,z} \\ M_{L,x}^A \\ M_{L,y}^A \end{bmatrix} + \frac{\tau_1}{\mathrm{J}_{21}} [\mathrm{J}_{2,2,\ldots,13}]^T. \tag{20}$$

As the biped is overactuated, a special attention must be given to the force distribution in the locomotion system to prevent undesirable antagonistic efforts that could provoke destabilizing effects, such as a break in the feet–ground contact. The approach that will be discussed next consists in the minimization of all active forces. The goal is to find a solution capable of handling these antagonistic efforts.

Let $\mathbf{F_A} = (u_2, \ldots, u_{13}, F_{L,x}, F_{L,z}, M_{L,x}^A, M_{L,y}^A)^T$ be the unknown acting inputs vector. Equation (20) can be concisely rewritten under the form

$$\tau_{\mathbf{A}} = \mathbf{J_A}\, \mathbf{F_A}, \tag{21}$$

https://doi.org/10.1017/S0263574710000287 Published online by Cambridge University Press

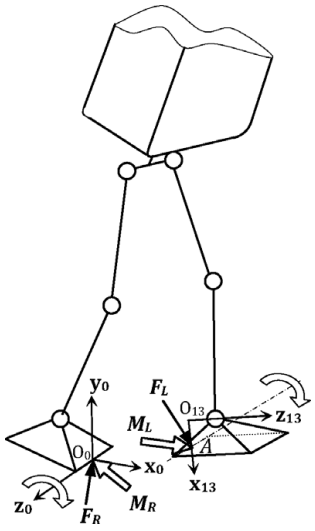


Fig. 5. Forces and moments applied on the feet during the DSP.

where $\tau_{\mathbf{A}}$ is a vector depending on actuating torques in the spanning tree system, given by

$$\tau_{\mathbf{A}} = \begin{bmatrix} \tau_2 \\ \vdots \\ \tau_{13} \end{bmatrix} - \frac{\tau_1}{\mathrm{J}_{21}} [\mathrm{J}_{[2,2,\ldots,13]}]^T, \tag{22}$$

whereas $\mathbf{J_A}$ is the 12×16 control inputs matrix defined as the concatenation of three matrices, namely

$$\mathbf{J_A} = \left[\mathbf{I}_{12\times12}\ [\mathrm{J}_{[1,2,\ldots,13]}]^T\ [\mathrm{J}_{[3,\ldots,5,2,\ldots,13]}]^T\right], \tag{23}$$

where $\mathbf{I}_{12\times12}$ denotes the 12×12 identity matrix.

Expression (21) represents a linear equation system having 16 unknowns (the $\mathbf{F_A}$ components) and 12 equations. Thus, among the infinity of solutions to the underdetermined system (21), a minimal quadratic-norm of the acting inputs $\mathbf{F_A}$ solution is given by the following expression:

$$\mathbf{F_A} = \mathbf{J_A^+}\ \tau_{\mathbf{A}}, \tag{24}$$

where $\mathbf{J_A^+}$ is the Moore–Penrose pseudo-inverse (see e.g., ref. [31]).

Since only the tangential components of contact reaction (see $\mathbf{F_A}$ components) are minimized by the expression (24), the nonsliding condition in Eq. (39) for the front foot during the DSP is easily satisfied.

Thereafter, the biped is considered freed from its front foot ground contact where known external forces are applied in order to keep its heel in their assigned contact positions as illustrated in Fig. 5. The vectors $\mathbf{F_L}$ and $\mathbf{M_L^A}$ are expressed in the local link coordinate frame, using the rotation matrix ${}^{13}\mathbf{R}_0$, such that

$$\begin{cases} {}^{13}\mathbf{F_L} = -{}^{13}\mathbf{R}_0\ \mathbf{F_L} \\ {}^{13}\mathbf{M_L^{O_{13}}} = -{}^{13}\mathbf{R}_0\ \mathbf{M_L^A} + \overrightarrow{\mathrm{O_{13}A}} \times {}^{13}\mathbf{F_L} \end{cases} \tag{25}$$

to be included in the inward recursions of the RNEA as external wrench. Consequently, the force $\mathbf{F_i}$ and the moment $\mathbf{M_i}$, that the $(i-1)$st link exerts on the ith link ($i=13$ to 1), are readily computed. This is the case for the force $\mathbf{F_R} = {}^0\mathbf{R}_1(q_1)\,\mathbf{F_1}$ and moment $\mathbf{M_R^{O_0}} = {}^0\mathbf{R}_1(q_1)\,\mathbf{M_1^{O_0}}$ applied at the toe of the rear foot by the ground with respect to the fixed base frame.

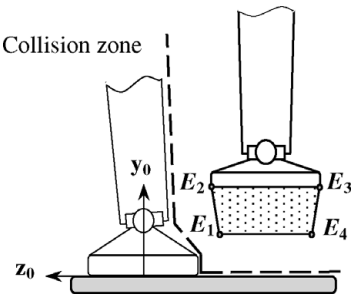


Fig. 6. Anticollision zone for the SSP.

As a result, both feet reaction wrench and the actuating torques are determined knowing the configuration vector $\mathbf{q}$, and its first two time-derivatives $\dot{\mathbf{q}}$ and $\ddot{\mathbf{q}}$.

4. Constraints Defining a Feasible Walk

Defining the constraints is the only way to express all the issues involved in the biped gait. Thus, a set of constraints is imposed in order to ensure the feasibility of the walking. We distinguish two subsets of constraints that a feasible step must obey.

4.1. Kinematic constraints

4.1.1. Bound constraints. The variation range of joint coordinates and active joint velocities is bounded, respectively, by setting

$$\forall t \in [0, t_S], \quad q_i^{min} \le q_i(t) \le q_i^{max}, \quad i = 1, \ldots, 16, \tag{26}$$

$$\forall t \in [0, t_S], \quad |\dot{q}_i(t)| \le \dot{q}_i^{max}, \quad i = 2, \ldots, 16, \tag{27}$$

where q_i^{min} and q_i^{max} are, respectively, the lower and the upper range motion bounds of joint i, and $\dot{q}_i^{max}$ is the maximum speed of joint i.

4.1.2. Swing foot collision avoidance. During the SSP, the motion must be organized in order to avoid collision between the swing foot and the ground as well as between both legs as shown in Fig. 6.

Ground collision avoidance: The swing foot toe and heel must not collide with the ground. Let $\mathbf{E}_i$ be the swing foot sole edge i homogenous coordinates vector into its own coordinate frame, and ${}^0\mathbf{T}_{13}$ the 4×4 homogeneous transformation matrix from the swing foot coordinate frame to the base one, the swing foot/ground anticollision conditions are such that

$$\forall t \in [0, t_{SS}], \quad [{}^0\mathbf{T}_{13}(\mathbf{q_C})\,\mathbf{E}_i]^T . \begin{bmatrix} 0 \\ 1 \\ 0 \\ 0 \end{bmatrix} \ge 0, \quad i = 1, \ldots, 4. \tag{28}$$

https://doi.org/10.1017/S0263574710000287 Published online by Cambridge University Press

Feet collision avoidance: The trajectory of the swing foot should avoid a forbidden zone enclosing the stance leg. This constraint can be written in the form

$$\forall t \in [0, t_{SS}], \quad \delta(x, y) - \mathbf{E}_{i,z} < 0, \quad i = 1, 2, \tag{29}$$

where $\mathbf{E}_{i,z}$ is the Z-coordinate of the point $\mathbf{E}_i$ and $\delta(x, y)$ the parametric function of the obstacle boundary.

4.1.3. Complementary constraints at phase transitions. The cyclic and bilaterally symmetric straight-ahead walking involves relationships between forces and motions at the beginning and at the end of the step. Thus, the joint coordinates at initial and final posture relationships are implicitly fulfilled thanks to the introduction of free parameters set (12) defining the transition postures. To complete the relationship between the initial and the final system states, the independent joint velocity equalities are stated as follows:

$$\begin{cases} \dot{q}_2(t_S) = \dot{q}_{13}(0), \\ \dot{q}_3(t_S) = -\dot{q}_{12}(0), \\ \dot{q}_4(t_S) = -\dot{q}_{11}(0), \\ \dot{q}_5(t_S) = -\dot{q}_{10}(0), \\ \dot{q}_6(t_S) = \dot{q}_9(0), \\ \dot{q}_7(t_S) = \dot{q}_8(0), \\ \dot{q}_{14}(t_S) = -\dot{q}_{14}(0), \\ \dot{q}_{15}(t_S) = -\dot{q}_{15}(0), \\ \dot{q}_{16}(t_S) = \dot{q}_{16}(0). \end{cases} \tag{30}$$

The same equalities hold for accelerations, introduced also via explicit equality constraints. Moreover, if an impactless swing foot heel-touch is required, the closed-loop kinematic constraint must be fulfilled also at SSP end, i.e.,

$$[\mathbf{J}_{1,\ldots,5,1,\ldots,13}]\, \dot{\mathbf{q}}_{\mathbf{C}}(t_{SS}) = \mathbf{0}. \tag{31}$$

4.2. Dynamic constraints

4.2.1. Actuating torque limitations. The joint actuating torques are bounded by setting

$$\forall t \in [0, t_S], \quad |u_i(t)| \le u_i^{max}, \quad i = 2, \ldots, 16, \tag{32}$$

where u_i^{max} denotes the ith joint maximum torque.

4.2.2. Stability conditions. Contrary to the actuating torque limitations that are not mandatory because the optimization algorithm tends to minimize them, the stability, meaning a walk without falling, is imperative. The stability depends on the ground-foot contact forces and moments already calculated for both phases in Section 3.

ZMP conditions: The zero moment point (ZMP), denoted P, is the point on the ground where the moment generated by the reaction forces moments has no component along the horizontal axes. It results in the following equation:

$$\left(\mathbf{M}_{\mathbf{k}}^{P}\right)_{\mathbf{t}} = \left(\mathbf{M}_{\mathbf{k}}^{O_0} + \mathbf{F}_{\mathbf{k}} \times \overrightarrow{O_0 P}\right)_{\mathbf{t}} = \mathbf{0}, \quad k \equiv R, T, \tag{33}$$

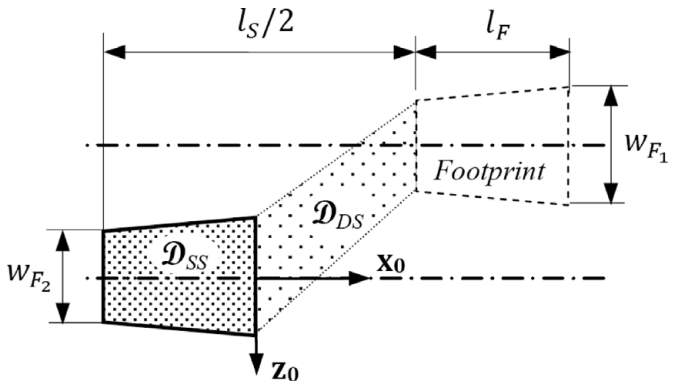


Fig. 7. Dynamically stable support polygon.

where the subscript $\boldsymbol{t}$ denotes the tangential component of vectors, and $\mathbf{F_T}$ and $\mathbf{M}_{\mathbf{T}}^{O_0}$ are respectively the total contact force and moment of both feet during the DSP at O_0, given by the formulas

$$\begin{cases} \mathbf{F_T} = \mathbf{F_R} + \mathbf{F_L}, \\ \mathbf{M}_{\mathbf{T}}^{O_0} = \mathbf{M}_{\mathbf{R}}^{O_0} + \mathbf{M}_{\mathbf{L}}^{A} + \overrightarrow{O_0 A} \times \mathbf{F_L}, \end{cases} \tag{34}$$

where $\mathbf{M}_{\mathbf{R}}^{O_0}$ and $\mathbf{M}_{\mathbf{L}}^{A}$ are the contact moments, respectively, at the rear foot toe and the front foot heel. To ensure the dynamic balance of the biped, the ZMP must be located inside the support polygon.[32] From Eq. (33), the ZMP coordinates during the SSP and the DSP are, respectively, given as follows:

$$\begin{cases} \forall t \in [0, t_{SS}], \ \overrightarrow{O_0 P} = \left(M_{R,z}^{O_0}/F_{R,y}, \ 0, \ -M_{R,x}^{O_0}/F_{R,y}\right)^T, \\ \forall t \in [t_{SS}, t_S], \ \overrightarrow{O_0 P} = \left(M_{T,z}^{O_0}/F_{T,y}, \ 0, \ -M_{T,x}^{O_0}/F_{T,y}\right)^T. \end{cases} \tag{35}$$

The support polygon or the convex hull of contact areas for each gait phase is shown in Fig. 7. The expressions of the dynamic balance conditions $\forall t \in [0, t_{SS}]$, $P \in \mathfrak{D}_{SS}$ and $\forall t \in [t_{SS}, t_S]$, $P \in \mathfrak{D}_{DS}$ are translated into the following inequalities:

$$\forall t \in [0, t_{SS}], \begin{cases} |P_x + l_F/2| - l_F/2 \le 0, \\ |P_z| - w_F/2 \le 0, \end{cases} \tag{36}$$

$$\forall t \in [t_{SS}, t_S], \begin{cases} P_x \ge 0, \ P_x - b \le 0, \\ P_z + \dfrac{(w_D - w_S/2)}{b} P_x + w_{F_1}/2 \ge 0, \\ P_z + \dfrac{(w_S/2 + w_D)}{b} P_x - w_{F_1}/2 \le 0, \end{cases} \tag{37}$$

with $w_F = (w_{F_1} + w_{F_2})/2$, $b = l_S/2 - l_F$ and $w_D = (w_{F_1} - w_{F_2})/2$.

Nonsliding and unilaterality conditions: In presence of Coulomb friction, the nonsliding conditions, satisfied during the SSP for the stance foot (where sliding rotation is also forbidden) and during the DSP for both feet, are given,

https://doi.org/10.1017/S0263574710000287 Published online by Cambridge University Press

respectively, as follows:

$$\forall t \in [0, t_{SS}], \quad \mu F_{R,y} \geq \sqrt{F_{R,x}^2 + F_{R,z}^2} + \left|M_{R,y}^P\right|/\rho, \quad (38)$$

$$\forall t \in [t_{SS},\ t_S], \begin{cases} \mu F_{R,y} \geq F_{R,xz} = \sqrt{F_{R,x}^2 + F_{R,z}^2}, \\ \mu\ F_{L,y} \geq F_{L,xz} = \sqrt{F_{L,x}^2 + F_{L,z}^2}, \end{cases} \quad (39)$$

where μ denotes a given dry-friction coefficient depending on the materials in contact, and $\rho = 0.5\sqrt{l_F^2 + w_F^2}$ is the friction radius of the biped sole introduced to take into account an additional tangential force induced by the moment normal to the ground surface.

The inequalities (38) and (39) perform also the unilaterality of contact conditions stating that the vertical components of the ground reaction forces must remain positive.

4.2.3. Periodic conditions. A cyclic step must satisfy some conditions related to the foot-ground contacts. First, at the beginning and at the end of step, the ZMP is located, respectively, under the right foot-heel and the left one symmetrically to the foot sagittal axis, i.e.,

$$P_z(t_S) = -P_z(0) - w_S. \quad (40)$$

Second, at step end, the right foot is ready to leave the ground to become the swing foot of next step. This means that the contact forces and moments acting on it are equal to zero at this instant, namely

$$\mathbf{F_R}(t_S) = \mathbf{0},\ \mathbf{M_R^{O_0}}(t_S) = \mathbf{0}. \quad (41)$$

Finally, the contact forces and moments at step beginning are related to their counterparts at step end. Indeed, the forces are symmetric about inertial X-and Y-axes and antisymmetric about Z-axis, while contact moments are symmetric about inertial Z-axis and antisymmetric about X-and Y-axes. That is,

$$\begin{cases} F_{R,x}(0) = F_{L,x}(t_S), \\ F_{R,y}(0) = F_{L,y}(t_S), \\ F_{R,z}(0) = -F_{L,z}(t_S), \\ M_{R,y}^P(0) = -M_{R,y}^P(t_S). \end{cases} \quad (42)$$

In addition to the periodic conditions on motion variables (11) and (30), these conditions lead to a periodic time variation of actuating torques.

5. Parametric Optimization Problem Statement

5.1. Performance criterion and constraints

The problem to be solved consists of finding time-function vectors $\mathbf{q}(t)$, $\dot{\mathbf{q}}(t)$, and $\ddot{\mathbf{q}}(t)$ of desired reference joint motions. A solution must minimize a performance criterion and satisfy equality constraints (30), (31), and (40)–(42) together with inequality constraints (26)–(29), (32), and (36)–(39). The chosen performance criterion is the integral of the actuating torques quadratic-norm throughout the walking step. It is expressed as a weighted sum of two terms, respectively, for each gait phase:

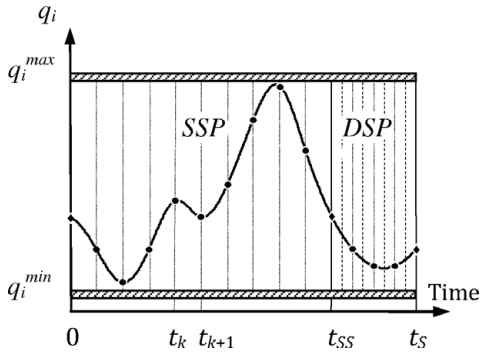


Fig. 8. Trajectory approximation using cubic spline interpolation at knots.

$$\mathrm{f}_{obj} = \alpha \int_0^{t_{SS}} \mathbf{u}(t)\,\mathbf{W}\,\mathbf{u}^T(t)\,dt + (1-\alpha)\int_{t_{SS}}^{t_S} \mathbf{u}(t)\,\mathbf{W}\,\mathbf{u}^T(t)\,dt, \quad (43)$$

where $\mathbf{W}$ a given diagonal matrix weighting the relative importance between actuating torques, by default, it is an identity matrix, and $\alpha \in [0, 1]$ is a coefficient weighing the relative importance of each phase in the minimizing problem.

This criterion has two beneficial effects. First, it is a continuous function of optimization parameters. Second, such a criterion will tend to generate upright walking patterns which require little effort to support gravity forces.

5.2. Parameter optimization problem stating

The trajectory parametrization is the solution to use efficient direct numerical methods for solving the optimal control problem. Moreover, the parametrization makes easy the modification of pre-calculated trajectories to apply them to slightly different situations by the control system. As shown in ref. [33], low-order piecewise polynomials such as the cubic spline functions bring several advantages.

Except for the front leg joint coordinates during the DSP, deduced from the closure conditions (1), (4), and (7), the joint coordinates are approximated by cubic spline functions. The optimization parameters are then the values of these functions at knots uniformly distributed along the motion time as shown in Fig. 8. The joint velocities and the accelerations are deduced from cubic splines proprieties. For each gait phase, knots may be chosen uniformly distributed along the time history. Let N_{SS} and N_{DS} be the number of knots introduced to parameterize the SSP and DSP joint trajectories, respectively. The number of new optimization parameters, namely the values of $q_i(t_k)$, amounts to $15(N_{SS} - 2)$ and $10(N_{DS} - 2)$ for both SSP and DSP, respectively. Setting

$$\begin{cases} \mathbf{x}_{SS} = \{q_i(t_k),\ i = 2, \ldots, 16,\ \ t_k \in]0, t_{SS}[\ \}, \\ \mathbf{x}_{DS} = \{q_i(t_k),\ i = 1 \ldots, \ldots, 7, 14, 15, 16, t_k \in]t_{SS},\ t_S[\ \}, \end{cases} \quad (44)$$

https://doi.org/10.1017/S0263574710000287 Published online by Cambridge University Press

and accounting for the transition configuration parameters defining $\mathbf{x}_B$ in (12), the complete set of optimization design parameters can be gathered in a single vector

$$\mathbf{x} = (x_1, \ldots, x_{n_P})^T = (t_{SS},\ t_S,\ \mathbf{x}_B,\ \mathbf{x}_{SS},\ \mathbf{x}_{DS})^T. \quad (45)$$

Then interpolated joint coordinates take the form

$$i \leq n,\ q_i(t) \cong \varphi_i(\mathbf{x}, t), \quad (46)$$

where φ_is are cubic spline functions of $\mathbf{x}$ and t. If we set

$$\varphi = (\varphi_1, \ldots, \varphi_{n_P})^T,\ \ \partial\varphi/\partial t \equiv \varphi_{,t},\ \ \partial^2\varphi/\partial t^2 \equiv \varphi_{,t^2}, \quad (47)$$

the vector $\mathbf{u}$ of actuating inputs must be explicitly formulated as a vector function of $\mathbf{x}$ and t. The vector-function $\mathbf{u}$ can be formally written as

$$\begin{aligned}\mathbf{u}(\mathbf{q}(t), \dot{\mathbf{q}}(t), \ddot{\mathbf{q}}(t)) &= \mathbf{U}(\varphi(\mathbf{x}, t), \varphi_{,t}(\mathbf{x}, t), \varphi_{,t^2}(\mathbf{x}, t)) \\ &\equiv \mathbf{U}(\mathbf{x}, t). \end{aligned} \quad (48)$$

In this way, the cost f_{obj} in (43) can be expressed as the following function of $\mathbf{x}$

$$\mathrm{f}_{obj}(\mathbf{x}) = \alpha\ \mathrm{f}_{SSP}(\mathbf{x}) + (1-\alpha)\ \mathrm{f}_{DSP}(\mathbf{x}). \quad (49)$$

The constraints in Section 4 depending on the running time t are accounted for at sufficiently close connecting times. Using the $\mathbf{x}$-representation of q_i and $\mathbf{u}$ in Eqs. (46) and (48), All the constraints can be easily reformulated as constraints depending on $\mathbf{x}$ that can be formally reformulate as

$$\begin{cases} C_j^I(\mathbf{x}) \leq 0, & j \leq N_{IC}, \\ C_k^E(\mathbf{x}) = 0, & k \leq N_{EC}, \end{cases} \quad (50)$$

where $C_j^I(\mathbf{x})$ and $C_k^E(\mathbf{x})$ stand for inequality and equality relation constraints, respectively, whereas N_{IC} and N_{EC} are their respective number.

5.3. Numerical Solving technique

The nonlinear minimization problem stated by the performance criterion (49) and the constraints (50) can be solved using Sequential Quadratic Programming (SQP) methods (an overview is found in ref. [34]).

The SQP, as all numerical optimization methods, provide a local minimum and are sensitive to the initial guess solution. To deal with the complexity of this minimization problem as well as the solving methods limitations, several stages of gait optimizations are performed with varying complexity. The constraints are introduced progressively in the optimization program and the solution is obtained by a succession of optimizations such that each succeeding optimization benefits from an initialization starting that is a previous optimal solution.

The routine *fmincon* of the *Matlab*® package optimization toolbox, which implements a SQP method, is used to solve the constrained nonlinear minimization. Depending on the initial guess solution, the computations, carried out on a 3 GHz *Pentium*® 4, took almost few hours.

6. Simulation Results

The simulations are essentially focused on the validation of the proposed method. The main kinematic and dynamic characteristics of the synthesized gaits as well as their differences with the sagittal gait model and the human walking features are highlighted to demonstrate its effectiveness.

The present method was applied for generating optimal cyclic steps of the 3D model of the anthropomorphic biped robot BIP,[16] which has a weight of 1030 N with a centre of gravity located at nearly one metre from the ground. Its modified DH parameters[24] and the inertial data are given in Table I.

The simulations were carried out for given walking speeds V that are related to the step duration and step length by the formula: $V = l_S/(2\ t_S)$. Table II summarizes the main results of several representative simulations concerning gaits with and without impact heel-touch. Besides, more detailed and interesting results are given for the impactless walk at $V = 0.5$ m/s and the walk with impact heel-touch at $V =$ 1 m/s.

6.1. Impactless walk at V = 0.5 m/s

The stick diagrams in Fig. 9 give an idea about how the gaits look. The motions are organized as expected: a SSP followed by a DSP. After the heel-touch both feet rotate around the heel and the toe, respectively. The obtained gait appears similar to a human being one except for the excessive angular rotation of the swing foot, during the SSP, due to its low contribution in the optimization criterion. The side view in Fig. 9(a) shows the supporting leg almost fully extended at mid-swing. It seems to move like an inverted pendulum. The trunk bends forward, affecting mostly the biped centre of gravity location in sagittal plane. In the front plane (Fig. 9(b)), the lateral motion of the stance leg is also that of an inverted pendulum around the stance ankle. However, the swing leg remains almost in the sagittal plane probably in order to reduce the gravity effect on its frontal hip joint torque. The Fig. 9(c) shows that the trunk remains nearly straight with low amplitude of the vertical rotation.

According to Fig. 9, it seems that the biped joints perform complex motions. Indeed, the graphs in Fig. 10 shows that all joints contribute to perform the walk. However, the variations of the sagittal plane joints (Figs. 10(a) and (c)), and in particular for the swing leg (Fig. 10(c)), are larger than those in the frontal plane (Fig. (b)) and the transverse plane (Fig. 10(d)). Figure 11 shows that the joint velocities are continuous over the step. Moreover, the motions in sagittal plane are clearly faster than in the other planes (Figs. 11(b) and (c)). Notice that actuators work at low speeds implying the possibility to take advantage of actuator torque amplification to improve the dynamic performances. The torque profiles in Fig. 12 are rough (not smooth). This feature comes from the linear acceleration profiles inherent to the cubic spline approximations of the independent joint coordinates. These jerky variations of actuating torques indicate also that walking dynamics is very depending from the joint accelerations.

The transverse joint torques as well as the waist joint torques evolve with quite small values during the walk. The

https://doi.org/10.1017/S0263574710000287 Published online by Cambridge University Press

Table I. Biped BIP geometrical dimensions and inertial data.

DH parameters						Mass (kg)		Mass center G_i			Inertia tensor I_{Gi} (kg · m^2)					
i	a_i	$\alpha_i\ (rd)$	$d_i\ (m)$	$q_i\ (rd)$	$r_i\ (m)$	i	m_i	G_{xi}	G_{yi}	G_{zi}	I_{xx}	I_{xy}	I_{xz}	I_{yy}	I_{yz}	I_{zz}
0	–	0	0	$\pi/2$	0	1	2.34	.024	.151	0	.02	0	0	0	0	0.02
1	0	$\pi/2$	.083	0	−.17	2	0.18	0	0	0	0	0	0	0	0	0.12
2	1	$-\pi/2$	0	0	0	3	5.93	.258	.028	0	.02	0	0	.07	0	0.29
3	2	0	.41	0	0	4	10.9	.25	.005	.045	.04	0	−.03	.12	0	0.63
4	3	0	.41	$\pi/2$	0	5	0.7	.002	−.034	0	0	0	0	0	0	0.63
5	4	$\pi/2$	0	$-\pi/2$	0	6	3.20	−.005	.107	.029	.02	0	0	0	.01	0.76
6	5	$\pi/2$	0	0	0	7	8.80	.11	−.012	−.068	.09	0	0	.09	.01	2.61
7	6	0	.22	0	0	8	3.20	.005	.029	−.107	.02	0	0	.01	−.01	2.57
8	7	$-\pi/2$	0	$\pi/2$	0	9	0.70	.002	0	.034	0	0	0	0	0	0.75
9	8	$-\pi/2$	0	$\pi/2$	0	10	10.9	.160	−.005	−.045	.04	0	−.03	.12	0	0.75
10	9	0	.41	0	0	11	5.93	.152	−.028	0	.02	0	0	.07	0	0.58
11	10	0	.41	0	0	12	0.18	0	0	0	0	0	0	0	0	0.22
12	11	$-\pi/2$	0	0	−.12	13	2.34	.059	0	.139	.02	0	0	.02	0	0.12
13	6	$-\pi/2$	.11	0	.128	14	1.05	0	.047	−.025	0	0	0	0	0	0.67
14	13	$\pi/2$	0	$\pi/2$	0	15	0.46	0	0	.046	.01	0	0	0	0	0.44
15	14	$-\pi/2$	0	0	0	16	48	.405	.013	0	1.2	.31	.11	2.87	0	3.84

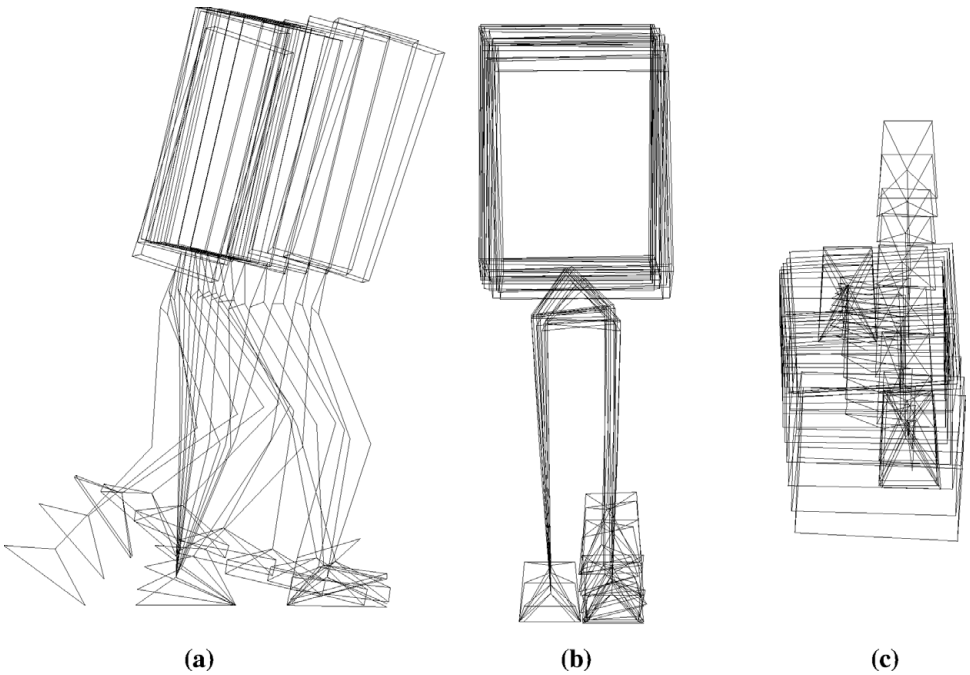
$\sigma_i = \gamma_i = \epsilon_i = 0, i = 1, 2, \ldots, 15.$

Table II. Main simulation results.

V(m/s)	**0.5**	**0.5**	**1.0**	**1.0**	**1.0**
V_{Impact}(m/s)	**0**	1.1	0	**4.32**	4.52
α	**0.5**	0.5	0.5	**0.5**	0.25
t_S	**0.88**	1.13	0.56	**0.47**	0.51
%DSP	**22**	24	33	**31**	33.5
f_{SSP}	**0.088**	0.202	0.153	**0.094**	0.178
f_{DSP}	**0.065**	0.148	0.176	**0.116**	0.099
f_{obj}	**0.077**	0.175	0.130	**0.105**	0.118

same observation is valid for the other actuating torques, during a great part of the SSP, except for the hip frontal torque u_7 (Fig. 12(b)) where the trunk is cantilevered. At the SSP end, u_7 diminishes rapidly simultaneously with the abrupt increase of actuating torques applied at ankle and at knee joints of the stance leg (u_3 and u_4, respectively). These high dynamic responses may be achievable using intermittent torque operations of actual brushless motors.[35]

During the DSP, the front leg joint torques augment at the beginning before their progressive decrease together with the other torques. Thus, at DSP end, as at SSP beginning, all actuating torques take very small values. Figure 13 shows



(a) **(b)** **(c)**

Fig. 9. Stick diagrams of the synthesized gait in: (a) sagittal plane; (b) frontal plane; (c) transverse plane.

https://doi.org/10.1017/S0263574710000287 Published online by Cambridge University Press

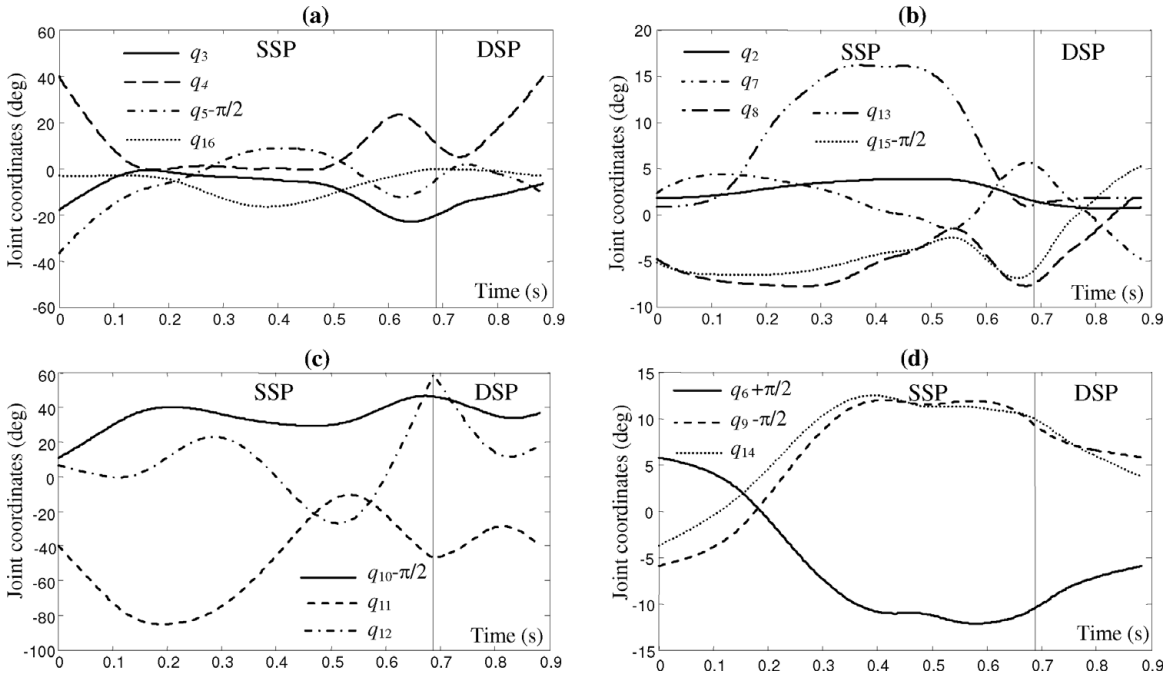


Fig. 10. Joint coordinates time variation.

the time evolution of the contact forces. The friction radius of the sole, ρ, and the dry-friction coefficient, μ, were set, respectively, at 0.165 and 0.6, knowing that in the case of rubber/concrete contact, typical values of μ vary between 0.5 and 0.9. With these set values, the no-slipping of the biped is guaranteed, particularly during the SSP, where the normal forces are noticeably higher than the tangential ones.

During the major part of the SSP, the normal contact force is equivalent to the biped weight except at the end of the swing where the normal reaction of ground contact exhibits a peak. During the DSP, the ratio, normal/tangential forces, diminishes denoting that during this phase the biped is less stable because of the risk of sliding. The rear foot can slide momentary at the end of the DSP. As for the actuating torques, at the DSP end and the SSP beginning, the normal contact forces are noticeably small. Figure 14 shows the ZMP locations and centre of gravity (CoG) trajectory projected on the ground during one cycle. The ZMP moves forward without jumps at phase transitions. As expected, the ZMP remains inside the support surface. During the SSP, for the most time, it is located under the ankle. During the DSP, the ZMP moves rapidly to positions in the front of the support

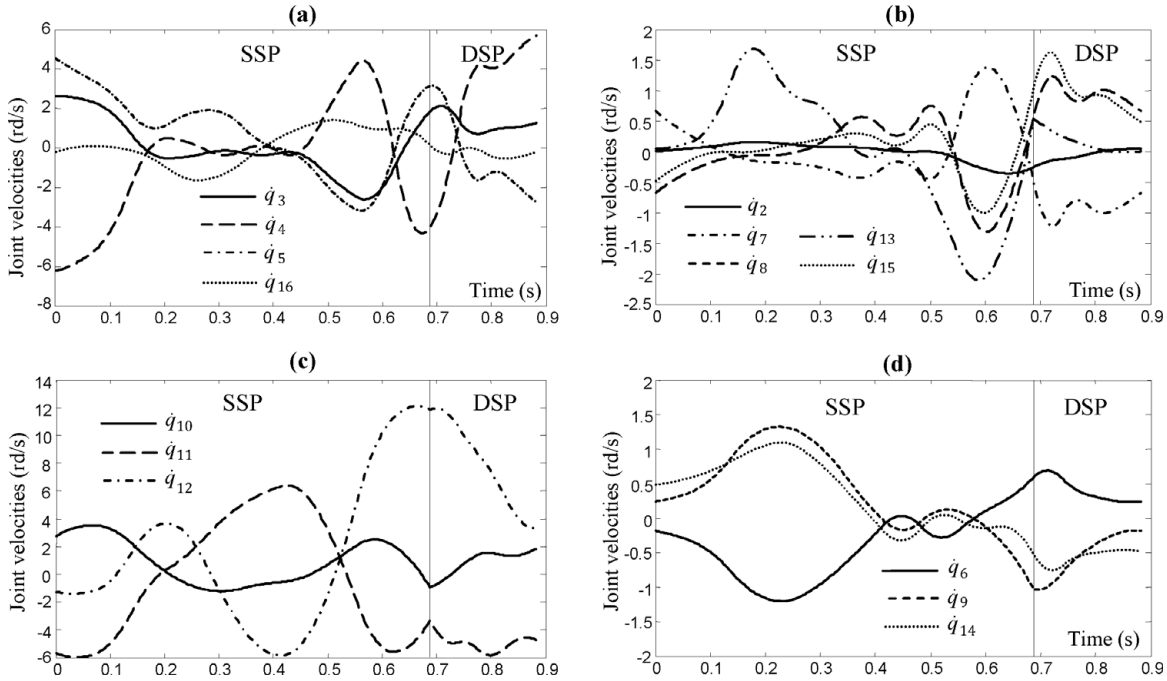


Fig. 11. Joint velocities time variation.

https://doi.org/10.1017/S0263574710000287 Published online by Cambridge University Press

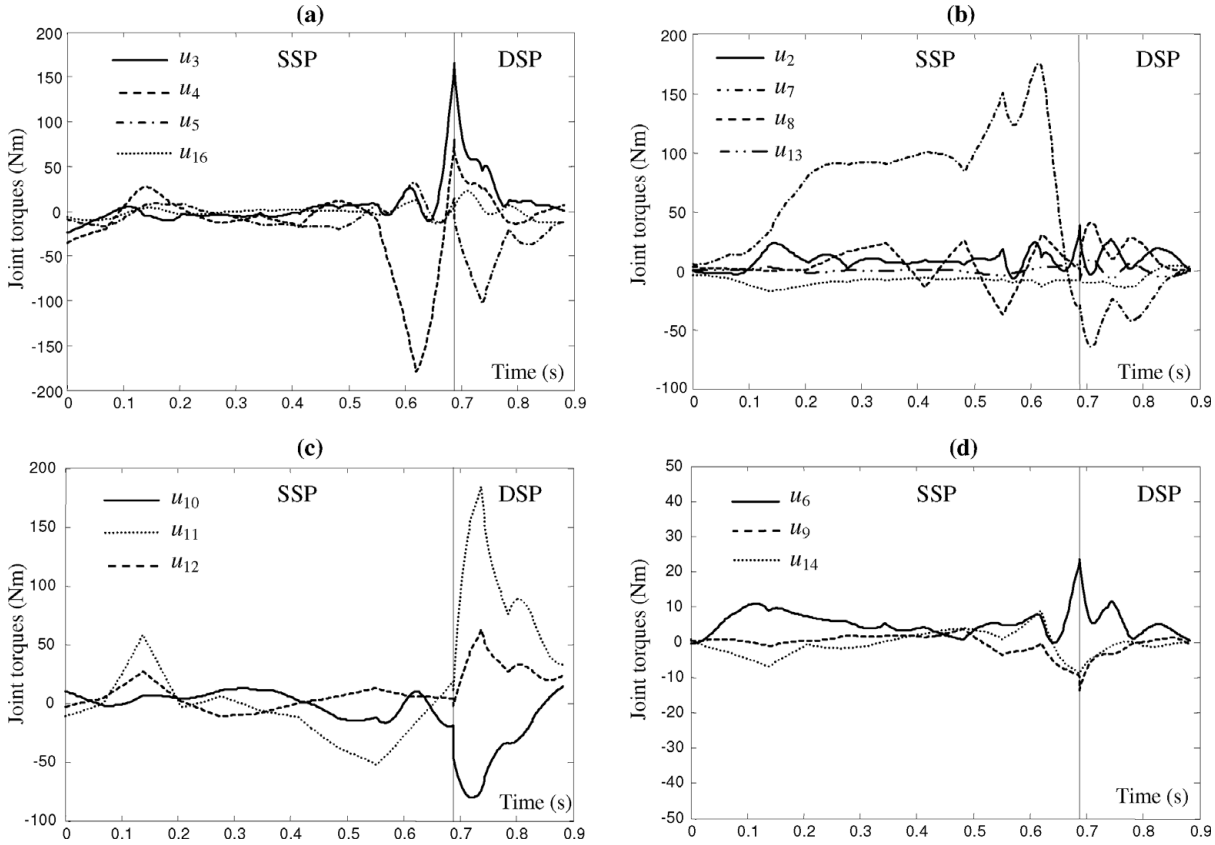


Fig. 12. Time variation of actuating joint torques at $V = 0.5$ m/s.

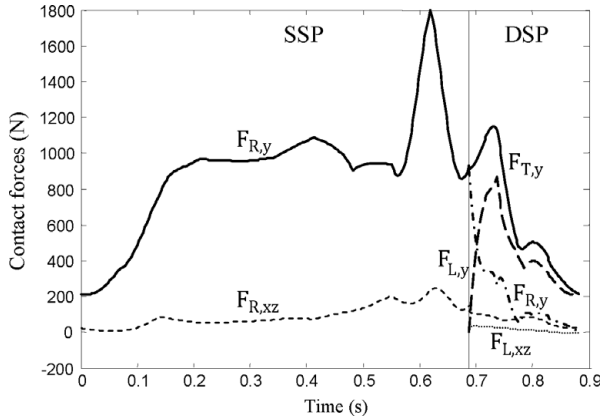


Fig. 13. Time variations of reaction forces at $V = 0.5$ m/s.

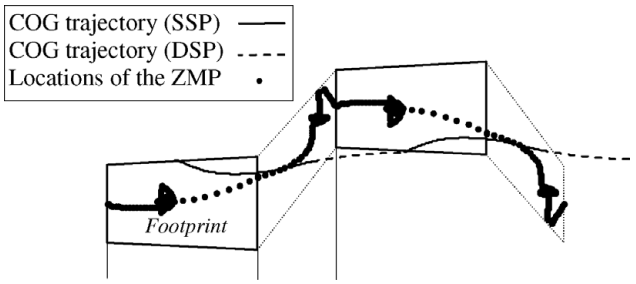


Fig. 14. ZMP trajectory and CoG projected on the footprints over one cycle.

area where it comes dangerously close to the stable area boundary; a falling down danger exists in addition to the sliding risk mentioned above.

6.2. *Walk with impact at heel-strike*

As shown in Table II, the increase of walking speed is achieved by a walking pace augmentation instead the step-length enlarging. Differently to the slow walk, walking with impacts at $V = 1.0$ m/s is more performant than impactless walk for both walking phases.

The modification in torques and contact forces evolution profiles relatively to the slow impactless walk is the expect discontinuity at phases transition. Furthermore, the torques are amplified (criterion value f_{obj} rises about 40%). Torques augmentation is due, first to the inertial forces (from motion accelerations) such as the torque u_8 acting on the frontal swing hip, second to the impact forces propagated to different joints such as the front leg knee and sagittal hip joints where the torque u_{10} and u_{11} increase suddenly at the DSP beginning to balance the impulsive impact force (see Fig. 15(c)). During a great part of the SSP, sagittal torques evolve with small values but they stay larger than in the case of the slow walk. The abrupt increase of the stance leg sagittal ankle torque u_3 persists while the stance knee torque u_4 does not rise at the SSP end, contrary to slow impactless walk. By inference, it seems that the torque u_4 has a contribution in the impactless heel-touch preparation.

Although the rise of actuating torques during the DSP, they evolve in the same manner than for the slow walk. The attempt to reduce torque magnitudes during the DSP by acting on the coefficient α (see the last column of Table II)

https://doi.org/10.1017/S0263574710000287 Published online by Cambridge University Press

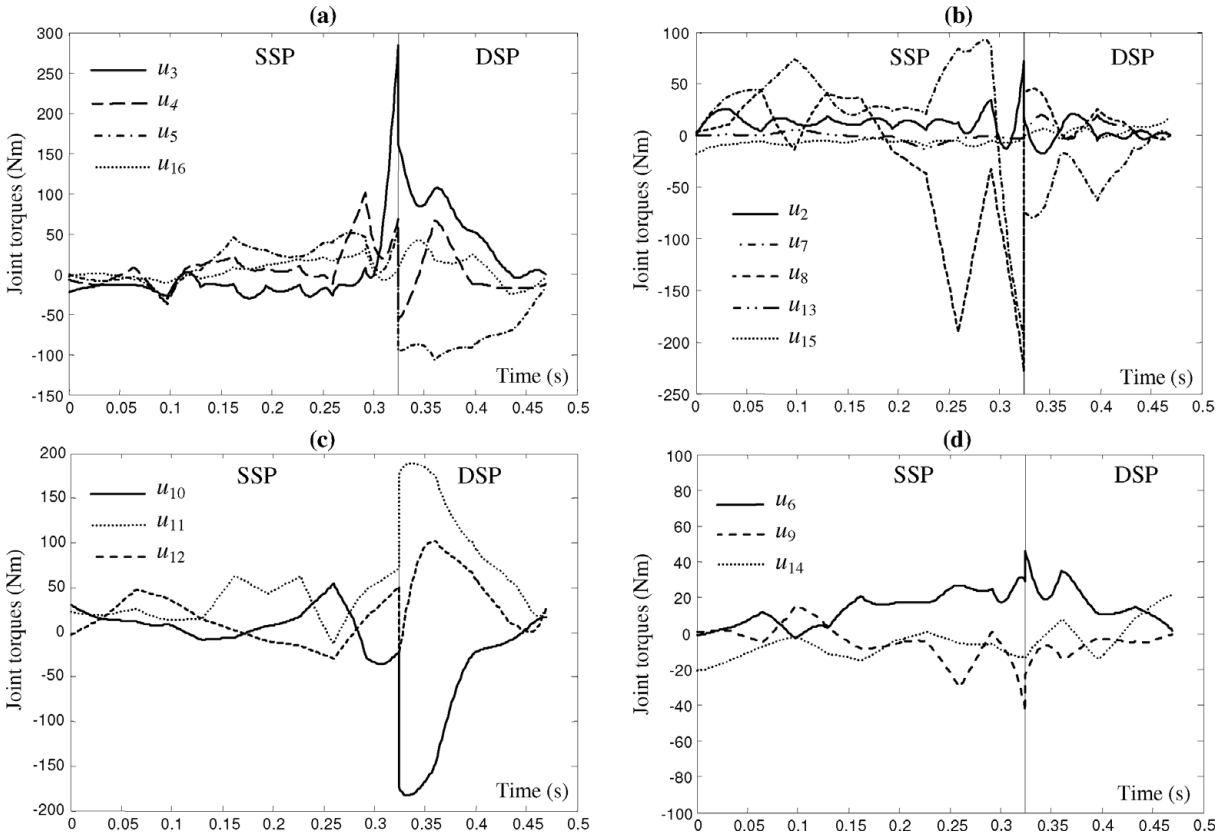


Fig. 15. Time variation of actuating joint torques at $V = 1$ m/s.

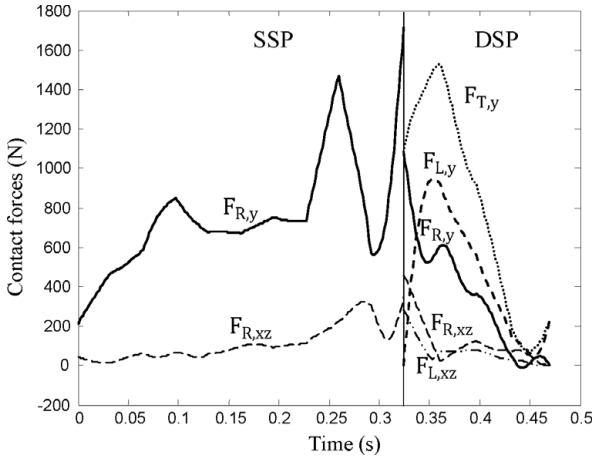


Fig. 16. Time variations of reaction forces at $V = 1$ m/s.

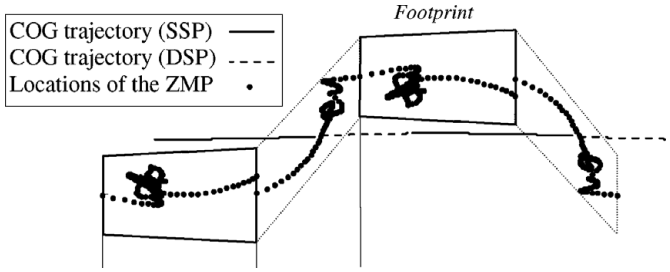


Fig. 17. ZMP trajectory, and COG projected on the footprints over one cycle at $V = 1$ m/s.

allowed to decrease slightly torque magnitudes during this phase but deteriorate the torque quality of the SSP. In fact, the coefficient α makes a compromise between the dynamics qualities of both phases and has not a direct effect on the stability.

As shown in Fig. 16, at the DSP ends, the walking tends toward a running because of the strongly diminution of normal forces. Figure 17 shows that the projected CoG trajectory has fewer oscillations compared to the slow walk one, while the ZMP moves forward with a small lateral jump at phase transitions. The evolution of ZMP and contact forces indicates that the remarks about the stability weakness during the DSP are still valid.

7. Discussion

The huge variations, observed through the simulations, in the evolution of torques and contact forces, clearly show the complexity of the dynamics of the walk.

In the case of small speeds, actuating torques evolve with quite small values during the major part of the SSP, showing a pendulum-like motion. Such a behavior is in agreement with the experimental results reported in ref. [36], indicating that there is a very little activity in the leg muscles during human walk at natural speed. The natural walking speed of this type of heavy biped robot is probably close to 0.5 m/s than to 1 m/s where the pendulum effect disappears.

At the end of the SSP, variations in several torque amplitudes occur. The abrupt increase of the sagittal stance ankle torque u_3 is notable in the case of both impactless and with impact heel-strike. It seems natural to assume that the optimal walk should include a stance foot rotation during the end of the SSP, which would cancel this ankle torque

https://doi.org/10.1017/S0263574710000287 Published online by Cambridge University Press

augmentation. However, the rise of the stance knee torque u_4 disappears in the case of impact heel-strike gaits. This torque tends to slowdown the swing motion in order to ensure impactless heel-touch. During the SSP, the ZMP location is far from boundaries, which indicates a certain stability margin, necessary from the practical point of view in order to recover minor disturbances in the control loop.[5]

The DSP should be given more attention because of the risk of contact break. The foot plantar flexion (which is a determinant for human biped, providing the propulsive effect) does not exist in the case of the biped robot. As a result, during the DSP, large actuating torques are required to initiate the support transfer between the feet. Nonetheless, thanks to the approach (in Section 3.2) used to solve the indeterminacy of the inverse dynamics, we achieve a well-balanced torque solution between leg joints.

According to the CoG trajectories, the synthesized gaits are dynamically balanced in agreement with the literature that admits the optimality of dynamic gaits on the static ones. The increase of walking speed makes the walk with impact heel-strike more efficient than the impactless gait as displayed in Table II. Nevertheless, it is necessary to attenuate the impact forces at heel-touch because of their impulsive effect on the joint torques.

The synthesized gaits exhibit some similarities with human walkers, such as the joint coordinate variations, the small values of the actuating torques during the major part of the SSP at natural gait speed and the order of magnitude of the actuating torques. However, torque evolution is quite different because the important characteristic of the human biped is the damping ability thanks to the simultaneous activation of antagonist muscles, which has not been taken into account in the rigid multibody model of the mechanical biped BIP. Moreover, fitting the joint trajectories using cubic spline functions may contribute to accentuating the difference. In other words, the anthropomorphic proprieties such as the masse repartition, the dimensions and the joint arrangement do not suffice to obtain the same torque evolutions.

In consequence, the simulation results show that the proposed approach succeeds in highlighting some issues but may be improved. First, as the approximation function features have great effects on the walking dynamics, it will be interesting to examine the effects of higher-order spline functions on gait characteristics. Second, other optimization methods can be investigated, such as stochastic search methods that would be more efficient to reach near-optimal solutions for such a complex problem. Finally, by introducing elastic links and subphases in the SSP and the DSP, simulation results will more closely match the human walk.

8. Conclusion

We proposed a general method synthesizing the cyclic gaits of three-dimensional biped models with up to 15 active joints. The walking step was generated by minimizing the quadratic norm of the joint torques under several physical constraints.

With minimum walking pattern knowledge, gaits were generated as a succession of SSPs finishing with or without an impactless heel-touch, which is consistent with DSPs. The walking cycle posture, the symmetry and the repeatability requirements as well as the DSP closure conditions were converted to a set of independent phase transition configuration parameters characterizing the SSP–DSP sequences.

During the SSP, the inverse dynamics problem was solved via an RNEA adapted to the kinematic tree-structures; whereas in the DSP, the proposed technique helps to overcome the underdeterminacy of the dynamic equations. The inverse dynamics problem was reformulated in such a manner as to minimize the norm of acting forces. The reaction forces on rear foot were accurately computed from the inward RNEA taking into account the forces applied on the front foot already computed.

The dynamics and the kinematics of the motion were subjected to limitations and conditions in order to get a feasible, stable, and well-organized gait patterns. These conditions are interdependent causing some difficulties to convert them into a number of constraints.

The simulation results have shown the possibilities of the proposed offline method to synthesize near-optimal three-dimensional walking patterns satisfying the whole walking constraints. The obtained gaits revealed several interesting features of the walking dynamics. Thus, the proposed method can be viewed also as a remarkable analysis tool.

Acknowledgments

I would like to express my gratitude to Guy Bessonnet and Philippe Sardain from Mechanics of Solids Laboratory, Poitiers University, France for making kinematic and dynamic characteristics of the biped robot BIP available for this work.

References

1. Honda Motor Co. Ltd., Honda Public relations Division, USA, "ASIMO-Technical Information," 1–34. (Sept. 2007). Available at http://asimo.honda.com/downloads/pdf/asimo-technical-information.pdf
2. K. Kaneko, K. Harada, F. Kanehiro, G. Miyamori and K. Akachi, "Humanoid Robot HRP-3," *Proceedings of IEEE/RSJ International Conference on Intelligent Robots and Systems*, Nice, France (2008) pp. 2471–2478.
3. F. Pfeiffer, "The TUM walking machines," *Phil. Trans. R. Soc. A* **365**, 109–131 (2007).
4. K. Hirai, M. Hirose, Y. Haikawa and T. Takenaka, "The Development of Honda Humanoid Robot," *Proceedings of IEEE ICRA*, Leuven, Belgium (1998) pp. 1321–1326.
5. Q. Huang, K. Kaneko, K. Yokoi, S. Kajita, T. Kotoku, N. Koyachi, H. Arai, N. Imamura, K. Komoriya and K. Tanie, "Balance Control of a Biped Robot Combining Off-line Pattern with Real-time Modification," *Proceedings of IEEE ICRA*, San Francisco, CA (2000) pp. 3346–3352.
6. H. Lim and A. Takanishi, "Compensatory motion control for a biped walking robot," *Robotica* **23**, 1–11 (2005).
7. C. Zhu and A. Kawamura, "Walking Principle Analysis for Biped Robot with ZMP Concept, Friction Constraint, and Inverted Pendulum Model," *Proceedings of IEEE/RSJ International Conference on Intelligent Robots and Systems*, Las Vegas, NV (2003) pp. 364–369.
8. H. Hirukawa, F. Kanehiro, K. Kaneko, S. Kajita, K. Fujiwara, Y. Kawai, F. Tomita, S. Hirai, K. Tanie, T. Isozumi, K. Akachi, T. Kawasaki, S. Ota, K. Yokoyama, H. Handa, Y. Fukase, J. Maeda, Y. Nakamura, S. Tachi and H. Inoue, "Humanoid robotics platforms developed in HRP," *Robot. Auton. Syst.* **48**, 165–175 (2004).

https://doi.org/10.1017/S0263574710000287 Published online by Cambridge University Press

9. T. McGeer, "Passive dynamic walking," *Int. J. Robot. Res.* **9**(2), 62–68 (1990).
10. S. Collins, A. Ruina, R. Tedrake and M. Wisse, "Efficient bipedal robots based on passive-dynamic walkers," *Science* **307**, 1082–1085 (2005).
11. M. G. Pandy and F. C. Anderson, "Dynamic Simulation of Human Movement using Large-Scale Models of the Body," *Proceedings of IEEE ICRA*, San Francisco, CA (2000) pp. 676–681.
12. P. H. Channon, S. H. Hopkins and D.T. Pham, "Derivation of optimal walking motions for bipedal walking robot," *Robotica* **10**, 165–172 (1992).
13. C. Chevallerau and Y. Aoustin, "Optimal reference trajectories for walking and running of a biped robot," *Robotica* **19**, 557–569 (2001).
14. M. Rostami and G. Bessonnet, "Sagittal gait of a biped robot during the single support phase. Part 2. Optimal motion," *Robotica* **19**, 241–253 (2001).
15. T. Saidouni and G. Bessonnet, "Generating globally optimized sagittal gait cycles of a biped robot," *Robotica* **21**, 199–210 (2003).
16. B. Espiau and P. Sardain, "The Anthropomorphic Biped BIP2000," *Proceedings of IEEE ICRA*, San Francisco, CA (2000) pp. 3997–4002.
17. T. Saidouni and G. Bessonnet, "Generating impactless gait of a bipedal robot," *Proceedings of the 11th World Congress in Mechanism and Machine Science*, Tianjin, China (2004) pp. 1532–1536.
18. G. Bessonnet, P. Seguin and P. Sardain, "A parametric optimization approach to walking pattern synthesis," *Int. J. Robot. Res.* **24**(7), 523–536 (2005).
19. T. Saidouni and G. Bessonnet, "A Simplified Method for Generating 3D Gait Using Optimal Sagittal Gait," *ROMANSY 16, Proceedings of the 16th CISM-IFToMM Symposium*, Warsaw, Poland (2006) pp. 195–202.
20. H. J. Kim, Q. Wang, S. Rahmatalla, C. C. Swan, J. S. Arora, K. Abdel-Malek and J. G. Assouline, "Dynamic motion planning of 3D human locomotion using gradient-based optimization," *ASME J. Biomech. Eng.* **130**, 031002-1–031002-14 (2008).
21. J. Denk and G. Schmidt, "Synthesis of Walking Primitive Databases for Biped Robots in 3D-Environments," *Proceedings of IEEE ICRA*, Taipei, Taiwan (2003) pp. 1343–1349.
22. M. Buss, M. Hardt, J. Kiener, M. Sobotka, M. Stelzer, O. Von Stryk and D.Wollherr, "Towards an Autonomous, Humanoid, and Dynamically Walking Robot: Modeling, Optimal Trajectory Planning, Hardware Architecture, and Experiments," *Third International Conference on Humanoid Robots*, Karlsruhe, Germany (2003).
23. O. Von Stryk, *User's Guide for DIRCOL Version 2.1*, Simulation and Systems Optimization Group, Technische Universität Darmstadt, [Online]. http://www.sim.informatik.tu-darmstadt.de/sw/dircol (2010).
24. W. Khalil and J. F. Kleinfinger, "A New Geometric Notation for Open and Closed-loop Robots," *Proceedings of IEEE ICRA*, San Francisco, CA (1986) pp. 1174–1179.
25. J. Y. S. Luh, M. W. Walker and R. Paul, "On-line computational scheme for mechanical manipulators," *ASME J. Dyn. Syst. Meas. Control* **102**(2), 69–76 (1980).
26. W. Khalil, J. F. Kleinfinger and M. Gautier, "Reducing the Computational Burden of the Dynamical Models of Robots," *Proceedings of IEEE ICRA,* San Francisco, CA (1986) pp. 525–531.
27. M. Nahon, "A comparison of methods for the control of redundantly-actuated robotic systems," *J. Intell. Robot. Syst.* **14**, 3–20 (1995).
28. H. Chaudhary and S. K. Saha, *Dynamics and Balancing of Multibody Systems* (Springer-Verlag, Berlin, 2009).
29. A. A. Shabana, *Dynamics of Multibody Systems*, 3rd ed. (Cambridge University Press, New York, 2005).
30. J. Angeles, *Fundamentals of Robotic Mechanical Systems: Theory, Methods and Algorithms*, 2nd ed. (Springer-Verlag, New York, 2003).
31. G. Strang, *Linear Algebra and its Applications*, 2nd ed. (Academic Press, London, 1980).
32. M. Vukobratovic and B. Borovac, "Zero-Moment Point–Thirty five years of it life," *Int. Humanoid Robot.* **1**(1), 157–173 (2004).
33. T. Saidouni and G. Bessonnet, "Gait Trajectory Optimization Using Approximation Functions," *Proceedings of the 5th International Conference on Climbing and Walking Robots*, Paris, France (2002) pp. 709–716.
34. R. Fletcher, *Practical Methods of Optimization*, 2nd ed. (John Wiley and Sons, Chichester and New York, 1987).
35. S. Lohmeier, T. Buschmann, H. Ulbrich and F. Pfeiffer, "Modular Joint Design for Performance Enhanced Humanoid Robot LOLA," *Proceedings of IEEE ICRA*, Orlando, FL (2006) pp. 88–93.
36. T. A. McMahon, "Mechanics of locomotion," *Int. J. Robot. Res.* **3**(2), 4–28 (1984).

https://doi.org/10.1017/S0263574710000287 Published online by Cambridge University Press